NASA TECHNICAL MEMORANDUM

NASA TM X-71594

NASA TM X-71594

INVESTIGATION OF THE STALL-INDUCED SHOCK WAVE (HAMMERSHOCK) AT THE INLET TO THE ENGINE

by Anatole P. Kurkov, Ronald H. Soeder,
and John E. Moss
Lewis Research Center
Cleveland, Ohio

TECHNICAL PAPER proposed for presentation at
Symposium on Propulsion System Structural
Integration and Engineering Integrity
Monterey, California, September 3-6, 1974

INVESTIGATION OF THE STALL-INDUCED SHOCK WAVE (HAMMERSHOCK) AT THE INLET TO THE ENGINE

by Anatole P. Kurkov*, Ronald H. Soeder**, and John E. Moss**
NASA Lewis Research Center, Cleveland, Ohio

E-8051

ABSTRACT

The peak static pressures measured at the inlet to the engine during stall are presented for a turbojet and two turbofan engines. It is shown for one turbofan and the turbojet that the static pressure ratio across the hammershock does not exceed significantly the normal shock pressure ratio necessary to stop the flow. The second turbofan engine did not follow this rule. Possible reasons for the departure are discussed. For the two turbofan engines the influence of the stall method on the hammershock intensity has been investigated. Data related to the spatial distribution of pressure in the hammershock are also presented.

* Aerospace Engineer, Member of AIAA.
** Aerospace Engineer

NOMENCLATURE

a	=	speed of sound
C_p	=	specific heat at constant pressure
M	=	Mach number
P	=	total pressure
p	=	static pressure
T	=	static temperature
t	=	time
V	=	velocity
V_p	=	shock propagation velocity
γ	=	specific heat ratio
ρ	=	density

Subscripts

1	=	airflow measuring station
2	=	engine inlet
3	=	compressor exit, J85 and GE 1/10
4	=	compressor exit, TF30
F	=	fan duct
H	=	maximum pressure in the hammershock
S	=	calculated pressure behind the shock wave

Superscripts

$\bar{}$	=	circumferential average
$\hat{}$	=	average of peak values
$'$	=	specific value of P used to normalize P_2 in Fig. 10.

INTRODUCTION

This paper is concerned with the description and correlation of the strength of the compression wave (hammershock) formed at the engine face immediately following stall. Peak pressure at the engine face as a result of compressor stall often exceeds by a wide margin the inlet total pressure. Therefore, accurate knowledge about the maximum possible value for this pressure is important as it provides the basis for calculation of the design-limiting pressures throughout the inlet system.

In addition to the maximum pressure in the hammershock, it is also important to have information about the magnitude of the pressure difference in the circumferential direction. This pressure difference acts as a lateral load on such inlet structures as the centerbody support struts and the inlet guide-vanes.

Previous experimental correlations of the peak pressure in the hammershock were usually given in terms of overall compressor pressure ratio. Using flight data on a two-spool turbofan engine (TF30), it was shown in Ref. 1 that the ratio of peak static pressure at the engine face to the compressor discharge static pressure is nearly independent of the compressor pressure ratio. In Ref. 2, this pressure-ratio correlation was applied to a turbojet engine with modification which amounted to the replacement of static pressures at the compressor inlet and discharge with total pressures.

References 3 and 4 correlate pressure ratio across the hammershock directly in terms of compressor pressure ratio. In Ref. 3, all pressures

were static and in Ref. 4, all pressures were total. Reference 4 also correlates peak total pressure at the compressor face in terms of compressor mass-flow at initiation of stall.

Reference 5 attempts to correlate the data from several engines in terms of a parameter which is a function of the maximum pressure rise across the hammershock, the engine inlet pressure, and the engine inlet Mach number.

In most of the reported work cited above, only one or two methods were employed to stall the engine. The question therefore remains as to whether the reported peak hammershock pressures could be exceeded if another method were chosen to stall the engine. Different stall methods may cause initiation of stall at different locations in a compressor and, therefore, have some influence on the intensity of the hammershock wave.

There also appears to be a need for a better correlation of the hammershock data from different engines. The data obtained at Lewis on a turbojet and two turbofan engines with different bypass ratios do not follow the trend predicted in Ref. 5.

The present investigation deals with the above two problems. Existing correlations are also examined as to their relative merit. Additional data are presented which examine the circumferential uniformity of the hammershock wave.

A low bypass ratio two-spool turbofan (TF30-P3), a higher bypass ratio two-spool turbofan (GE 1/10), and a turbojet (J85-13) are included in the investigation. The data from the first engine were obtained by employing nine different stall methods. The second and third engines involved, respectively, five and two different stall methods. A wide range of operating conditions are covered for each engine. The tests include several types of inlet flow distortion of varying extent.

The data on all three engines were obtained in a direct-connect type altitude test facility.

APPARATUS AND PROCEDURE

Engines Investigated

Figure 1 illustrates the three engines investigated with associated inlet ducting. The TF30-P3 and GE 1/10 engines are both two-spool turbofans with respective bypass ratios of 1.0 and 1.5. The TF30 engine has a three-stage fan and a six-stage axial compressor on the low-speed spool and a seven-stage axial compressor on the high-speed spool. The GE 1/10 engine has a two-stage fan on the low-speed spool and a seven-stage axial compressor on the high-speed spool. The fan and compressor in this engine are not as closely coupled as in the TF30 engine.

The J85-13 engine is a single spool turbojet. The eight-stage axial compressor in this engine is equipped with variable inlet guide-vanes. All three engines are equipped with afterburners.

Also shown in Fig. 1 are the locations of the distortion devices for each engine. The numbers in the figure designate the locations of: airflow measuring station (1), engine inlet station (2), and compressor discharge station (3 or 4).

Engine Stall Methods

The following methods were employed to stall the TF30 engine:

1. Sudden introduction of a premetered quantity of fuel to the primary burner (fuel-pulse);
2. Gradual introduction of air into the high-pressure compressor discharge volume (inflow-bleed);
3. Slowly advancing the engine throttle in conjunction with an off-design nozzle area setting (acceleration);
4. Gradually increasing the exit nozzle area;
5. Inducing afterburner transients; and,
6. Inducing inlet flow distortion.

Methods (1) to (4) result in either an increase of the compressor discharge pressure until the engine stalls (1), or a rematch among the various engine components eventually causing stall (3,4), or a combination of both (2). Afterburner transients involving both, throttle bursts and throttle chops result in a pressure rise in the afterburner (Ref. 6).

Inlet flow-distortion stalls involved both pressure and temperature distortions. Pressure distortions were produced by an air-jet system installed in front of the fan, facing upstream (Ref. 7). A pressure distortion pattern was produced by flowing the secondary air through the jets forming the desired distortion pattern. The steady-state

pressure distortion stalls were obtained by gradually increasing the secondary air flow through the distorted sector, i.e., amplifying the distortion.

Dynamic pressure distortion stalls were generated by using the air-jet system to simulate the dynamic distortions pattern from the engine-inlet pressure records obtained during a flight of a F111A airplane (flight simulation stalls).

Temperature distortion was produced by a hydrogen burner located in front of the bellmouth, which was divided into four quadrants (Ref. 8). These quadrants could be fired independently or in combination with each other. The level of distortion was controlled by the hydrogen flow rate. Inlet temperature pulses were produced by a sudden introduction of a premetered quantity of hydrogen to the burner.

For the TF30 engine, the extent of the inlet temperature and pressure distortion was 180°, except for two inlet temperature pulses which involved the full 360° extent, and the three flight-simulation stalls which duplicated the F111 inlet distortion pattern.

Methods (1) through (5) noted previously for the TF30 engine were also used to stall the GE 1/10 engine. The difference being that the exit nozzle area had to be decreased and the afterburner transients were limited to afterburner ignition. Stalls produced by inlet flow distortion were not attempted with this engine. However, during most of the runs some flow distortion was present. The flow distortion was

generated by several different types of screens installed in front of the engine (Fig. 1). The GE 1/10 engine stalls are discussed more fully in Ref. 9.

The J85 engine was stalled by reducing the exhaust nozzle area and by initiating an inlet temperature pulse. As in the case of the TF30 engine, hydrogen burners were located in front of the inlet bellmouth (Fig. 1). Some inlet temperature distortion was always present. The distortion patterns involved combinations of one to three temperature-distorted quadrants. A few temperature-pulse stalls involved all four quadrants. Temperature distortion effects on the J-85 engine are discussed more fully in Ref. 10.

Instrumentation

Specially designed probes and static taps utilizing miniature high-frequency response transducers (Ref. 11) were used to measure transient pressures at various locations in the engine. The analog pressure records of the stalls were digitized and converted to engineering units. The rate of digitization was every millisecond for the TF30 and J85 engines and every 10 milliseconds for the GE 1/10 engine. For the latter engine, therefore, analog pressure records had to be used in order to locate the maximum inlet pressure during stall.

The high-response pressure instrumentation located at station 2 (Fig. 1) included two static and 40 total pressures for the TF30 engine, two static and two total pressures for the GE 1/10 engine, and four static pressures for the J85 engine. In all cases static pressures were located in the outer wall of the annulus,i.e., tip wall.

At least one high-response compressor-discharge static pressure was available for each engine. For the TF30 and GE 1/10 engines use was also made of two static pressure measurements behind the rear fan stage in the bypass duct and the core compressor inlet. During some of the tests on the TF30 engine, a high-response static pressure was also recorded at station 1 (Fig. 1).

RESULTS

Correlation of Peak Hammershock Pressures in Terms of Pressure Ratios

Figure 2 presents peak static pressure ratios across the hammershock plotted against the static pressure ratio across the compressor for the TF30 engine. The peak static pressure in the hammershock is the larger maximum value recorded by the two pressure transducers at station 2. The values of engine-inlet and compressor-discharge static pressures used in Fig. 2 were obtained from digitized analog records at some point in time usually within 75 milliseconds prior to the first indication of stall. The choice of time relative to stall when these pressures are read is especially significant for the fuel-pulse stalls. The application of a fuel pulse often resulted in a marked compressor discharge pressure rise within about 60 milliseconds of stall. Two values for this pressure are therefore possible. One value corresponds to the steady-state level preceding the fuel pulse, and the other value corresponds to the post fuel-pulse level, usually taken within 30 milliseconds preceding the stall. In Fig. 2 the data are plotted based on both pre- and post- fuel-pulse levels (open and shaded symbols, respectively). To a lesser degree engine pressures were also affected by the afterburner transients. A small rise in both compressor discharge and engine-inlet static pressure was noticed following an afterburner transient. In Fig. 2 these points were, therefore, treated in the same way as the fuel pulse points.

For some fuel-pulse stalls it appears that a steady-state condition was not established prior to the stalling fuel-pulse. This was particularly evident in the case of the flagged points noted in Fig. 2 which fell considerably below all other points. (To be consistent with the general rule stated previously, in such cases pressures were read at about 75 milliseconds preceding the stall for points using pre-pulse pressures.) These points were included in order to illustrate the importance of having a steady pressure level at the compressor exit when using this correlation. As will be shown, this requirement is not nearly as critical when correlating hammershock pressures in terms of another parameter.

The fuel-pulse and afterburner-transient points corresponding to post-pulse values of the pressure ratios, shown as shaded symbols in Fig. 2, are displaced to the right (fuel pulses) or below (afterburner transients) their pre-pulse positions. In particular, fuel-pulse points are seen to fall considerably below all the other points. This seems to indicate that the compressor has not adjusted to the higher exit pressure level induced by a fuel pulse and that, therefore, when using this correlation for the TF30 engine the compressor discharge pressure should correspond to the pre-pulse level.

In general, a fair amount of data scatter can be noticed in Fig. 2 even if flagged and post- fuel-pulse points are excluded from consideration. However, for any one particular stall method, except possibly for fuel pulses, a considerably narrower data scatter band can be defined. It can be seen that, in general, distortion generated stalls produce higher peak hammershock pressures than stalls generated by other methods. The upper limit for the hammershock pressure ratio is determined by the steady-state pressure-distortion stalls.

The results for the GE 1/10 engine are shown in Fig. 3. As in the case of the TF30 engine, there is considerable data scatter and the post-fuel-pulse

points fall to the right of their respective pre-pulse positions. However, in the case of the GE 1/10 engine, the fuel-pulse points deviate less from the rest of the points if the pressure ratios are taken to correspond to post-fuel-pulse levels. The upper limit of the hammershock pressure ratios in Fig. 3 is defined by fuel-pulse points.

The results for the J85 engine are presented in Fig. 4. In comparison with previous figures, there appears to be less scatter. In part, this may be due to the fact that the J85 is a relatively simple engine in comparison with the TF30 and GE 1/10 engines. However, this may also be due to the fact that only two stall methods were employed for this engine.

Results from all three engines are compared in Fig. 5. In addition, this figure includes flight data from the TF30-P1 engine reported in Ref. 1, and data on the Olympus 593 B engine reported in Ref. 3. It can be seen that each engine spans about the same range of hammershock pressure ratios, and that different engines, in general, do not correlate with each other.

The flight stall data from the TF30-P1 engine result in somewhat stronger hammershocks at higher pressure ratios than indicated by the present data on the TF30-P3 engine. It was indicated in Ref. 1 that the most prominent cause of compressor stall was steady-state distortion. The stall data obtained from the altitude test facility which most closely approach the flight data are also obtained by steady-state distortion. However, referring to Fig. 2, it can be seen that dynamic flight-simulation points fell considerably below the flight data.

Additional data on the J85 engine tested in combination with a supersonic inlet are reported in Refs. 2 and 4. However, in these references total pressures rather than static pressures were used to correlate the data. Neglecting small differences between total and static pressures, the agreement with the data presented in Figs. 4 and 5 is good except at low pressure ratios where several points reported in Ref. 4 would fall below the lower

line indicated in Figs. 4 and 5.

In Figure 6 the maximum static pressure in the hammershock was ratioed to the compressor discharge static pressure. It was noted in Ref. 1 that the peak hammershock pressure normalized in this way is fairly independent of the compressor pressure ratio. As seen in Fig. 6 this does not seem to hold for the present data. For consistency with the TF30 engine, the data for the GE 1/10 engine in Fig. 6 were plotted using pre-fuel-pulse compressor-discharge pressures.

Figure 7 presents another correlation for the GE 1/10 engine. Hammershock static pressure ratio is plotted against the fan duct to engine inlet static pressure ratio. It is seen that the data scatter is reduced in comparison with Fig. 3. For the TF30 engine, however, no improvement has been noticed using this correlation.

Characteristics of Hammershock Wave and Dependence on Engine Inlet Mach Number

When relating the static pressure ratio across the hammershock to the engine inlet Mach number, it is also of interest to compare the measured pressure ratios with calculated pressure ratios across the shock wave for which the flow velocity behind the wave is zero. Occasionally, such a comparison has been made using isolated data points (Refs. 12 and 13). Results were, however, often conflicting.

Simple expressions can be derived for the flow-stoppage shock-propagation velocity and pressure ratio. Use is made of one-dimensional conservation equations for mass, momentum, and energy across the shock wave:

$$\rho_2 (V_2 + V_p) = \rho_s V_p$$

$$p_2 + \rho_2 (V_2 + V_p)^2 = p_s + \rho_s V_p^2$$

$$C_p T_2 + (V_2 + V_p)^2/2 = C_p T_s + V_p^2/2$$

The resulting expressions are:

$$V_p = a_2 \left\{ \sqrt{1 + \left[M_2(\gamma+1)/4 \right]^2} + M_2 \left[(\gamma+1)/4 - 1 \right] \right\} \quad (1)$$

$$(p_s/p_2) = 1 + \gamma M_2 \left\{ \sqrt{1 + \left[M_2 (\gamma+1)/4 \right]^2} + M_2(\gamma+1)/4 \right\} \quad (2)$$

where V_p is directed upstream.

The values of (p_s/p_2) calculated from Eq. (2) are plotted together with the measured hammershock pressure ratios in Fig. 8. The computed shock pressure ratio provides a faily good estimate of the upper bound of the experimental data, particularly at higher Mach numbers.

It can be seen that the four post-fuel-pulse points noted previously in Fig. 2 (flagged points) are now within the range of the other data points. This indicates that correlating the data in terms of inlet Mach number has practical advantages.

Figure 9 presents time histories of two static and two total engine inlet pressures approximately 180 degrees apart during the fuel-step stall corresponding to $M_2 = .444$ in Fig. 8. It is noted that on one side of the inlet duct the static pressure exceeds the total pressure, which indicates that in this part of the inlet duct, the flow is reversed. However, the differences between static and total pressures on either side of the duct are small compared to the pressure rise in the hammershock, which indicates why the one-dimensional theory gives good results. Also plotted in Fig. 9 is the static pressure at station 1 at a circumferential position of 288 degrees. Station 1 is 2.17 m (7.125 ft) upstream of station 2 and the time delay between the two pressure traces in Fig. 9 is about 7.8 milliseconds. The resulting hammershock propagation velocity is 278.4 m/sec (913.5 ft/sec), which is close to the value of 292.5 m/sec (959.6 ft/sec), obtained from Eq. (1). From the velocity of propagation obtained from Fig. 9, it follows that the wave on the 90 degree side of the duct leads the wave on the 270 degree side by about 47.3 cm (1.55 ft).

Upon passing through the duct the compression wave is reflected as a

rarefaction wave from the constant pressure boundary at the entrance to the bellmouth. As shown in Fig. 9, this wave is first observed at station 1 and then at station 2.

Additional information on the characteristics of the hammershock wave may be obtained from Fig. 10 in which the total pressure histories are traced at eight circumferential locations during an inflow-bleed stall. The total pressures in this figure are ratioed to their respective values at about 200 milliseconds prior to stall. The straight line in Fig. 10 indicates that corresponding pressure peaks appear to be displaced axially by an amount roughly corresponding to the time it takes the fan to traverse the angle between any two pressure traces being compared.

Figure 11 presents the correlation of the pressure ratio across the hammershock in terms of Mach number for the J85 engine. The Mach numbers for this figure are based on measurements with steady-state type instrumentation since there was no high-response total pressure instrumentation for this engine at station 2. However, only those points were plotted for which the steady-state compressor static pressure ratio was within three percent of the static pressure ratio evaluated from the high-response transducer measurements at the time of initiation of stall.

The predicted shock pressure ratio using Eq. (2) is exceeded by a wider margin for this engine than for the TF30 engine. The maximum deviation is about 7 percent for the point corresponding to $M_2 = .472$. Since the one-dimensional theory assumes uniform pressure circumferentially, it is possible that the departure between measured and predicted pressure ratios is partly due to the circumferential variation of pressure in the hammershock wave. The extent of the circumferential pressure nonuniformity in the hammershock is illustrated in Fig. 12 where four static pressure traces corresponding to four different angular positions are superimposed. In order to reduce the experimental hammershock data to an equivalent one-dimensional compression

wave, two averaging procedures can be used. One is simply taking the average of peak pressures recorded by each of the four static pressure transducers, and the other is taking the maximum of the average pressure, i.e., the four pressures are averaged at each millisecond and then the maximum pressure is selected. Figure 13 shows that the points which were above the curve in Fig. 11 are now below or only slightly above the curve when using the first procedure, and that using the second procedure all points fall below the curve. Therefore, at least on this latter basis, the calculated flow-stoppage pressure ratio remains the limiting pressure ratio.

The results for the GE 1/10 engine are presented in Fig. 14. It can be seen that several points fall considerably above the curve for zero-flow shock pressure ratio computed from Eq. (2). Averaging the two static pressure maxima brought two points fairly close to the curve; however, the other three points were affected very little. In an attempt to explain the reason for this departure, in Fig. 15 two neighboring engine inlet static/total pressure pairs were plotted for a fuel pulse point corresponding to $M_2 = .397$. The two total pressures were positioned radially fairly close to the duct wall, i.e., in the fan-tip region. It can be seen that the static pressures exceed total pressures by a much wider margin than in Fig. 9 for the TF30 engine. It appears that flow reversal in the fan-tip region for the GE 1/10 engine is much more pronounced than for the TF 30 engine. Examination of pressure traces at other stations in the engine shows that flow reversal in the fan-tip region is established prior to any indication of stall in the engine core flow. It is likely, therefore, that at the time of initiation of hammershock, flow has a positive direction in the fan-hub region, and a negative direction in the fan-tip region.

The presence of reversed flow in the hammershock, on an average basis, is also indicated by the one-dimensional theory. Equations (1) and (2) may be generalized for an arbitrary flow velocity behind the shock wave

as follows:

$$V_p = \sqrt{a_2^2 + \left[(V_2 - V_s)\ (\gamma + 1)/4\right]^2} + (V_2 - V_s)\ (\gamma + 1)/4 - V_2 \qquad (3)$$

$$(p_s/p_2) = 1 + \gamma\left(\frac{V_2 - V_s}{a_2}\right)\left[\sqrt{1 + \frac{1}{4}\left(\frac{V_2 - V_s}{a_2}\right)\left(\frac{\gamma + 1}{4}\right)}\right]^2 + \left(\frac{V_2 - V_s}{a_2}\right)\left(\frac{\gamma + 1}{4}\right) \qquad (4)$$

As can be seen from Fig. 14, shock pressure ratio computed from Eq. (4) with $V_s = -0.25V_2$, fairs very well the three points for which the averaged hammershock intensity is the highest.

It should be noted that part of the discrepancy observed in Fig. 14 may be also due to the difficulty in accurately determining the effective Mach number. Unlike the other two engines, the GE 1/10 engine was not equipped with a long bullet nose. Station 2 was, therefore, in the region of rapidly varying flow area.

The Mach numbers for Fig. 14, as in the case of the J85 engine, were obtained from steady-state type measurements. Because most of the data on the GE 1/10 engine were obtained with some screen distortion, the two available dynamic total pressure measurements did not provide sufficient coverage of flow area to obtain an average representative Mach number. Only those points were plotted for which the steady-state compressor static pressure ratio was within three percent of the dynamic static pressure ratio at initiation of stall.

In terms of engine inlet Mach number, the conclusion reached previously as to which stall method results in the strongest hammershock is modified somewhat. Considering only the stall methods attempted on both the TF30 and GE 1/10 engines, Figs. 8 and 14 each show that the strongest hammershocks are obtained as a result of stall caused by an afterburner transient or a fuel pulse. To these, inlet pressure-distortion stall must be added for the TF30 engine, as indicated in Fig. 8.

CONCLUSIONS

Experimental data on two engines, a turbofan and a turbojet show that the strongest hammershocks at the engine inlet correlate well with engine-inlet Mach number. The shock pressure ratio necessary to stop the flow, computed on the basis of engine-inlet Mach number, forms an upper bound for the observed pressure ratios across the hammershock based on maximum circumferentially averaged pressure at the inlet to the engine. The pressure ratio across the hammershock based on maximum pressure recorded at the engine inlet by any one pressure transducer does not exceed the flow-stoppage shock pressure-ratio by more than 7 percent.

Mach number correlation did not hold for the third engine, a turbofan in which fan-tip stall caused strong flow reversal in front of the engine near the duct wall.

On an individual engine basis, hammershock pressure ratio can be correlated in terms of compressor system static pressure ratio.

For a given engine-inlet Mach number the highest pressures at the engine inlet were obtained as a result of stall caused by inlet pressure - distortion, a fuel pulse, or an afterburner transient. For a given compressor pressure-ratio, inlet pressure-distortion stall produced the highest pressure at the engine inlet.

The highest engine-face static pressure during stall, taking into account all three engines, was about twice the engine inlet static pressure.

REFERENCES

1. Bellman, D.R., and Hughes, D.L., "The Flight Investigation of Pressure Phenomena in the Air Intake of an F111A Airplane," AIAA Paper 69-488, Colardo Springs, Colorado, 1969.

2. Choby, D.A., Burstadt, P.L., and Calogeras, J.E., "Unstart and Stall Interactions Between a Turbojet Engine and an Axisymmetric Inlet with 60-Percent Internal-Area Contraction", TM X-2192, March 1971, NASA.

3. Morriss, D.P., and Williams, D.D., "Free-Jet Testing of a Supersonic Engine/Intake Combination", Aeronautical Journal, Vol. 74, March 1970, pp. 212-218.

4. Mitchell, G.A., and Johnson, D.F., "Experimental Investigation of the Interaction of a Nacelle-Mounted Supersonic Propulsion System with a Wing Boundary Layer", TM X-2184, March 1971, NASA.

5. Marshall, F.L., "Predictions of Inlet Duct Overpressures Resulting From Engine Surge", AIAA Paper 72-1142, New Orleans, LA, 1972.

6. McAulay, J.E., and Abdelwahab, M., "Experimental Evaluation of a TF-30-P-3 Turbofan Engine in an Altitude Facility: Afterburner Performance and Engine-Afterburner Operating Limits", TN D-6839, July 1972, NASA.

7. Braithwaite, W.M., Dicus, J.H., and Moss, J.E., Jr., "Evaluation with a Turbofan Engine of Air Jets as a Steady-State Inlet Flow Distortion Device", TM X-1955, Jan. 1970, NASA.

8. Braithwaite, W.M., "Experimental Evaluation of a TF30-P-3 Turbofan Engine in an Altitude Facility: Effect of Steady-State Temperature Distortion", TM X-2921, Nov. 1973, NASA.

9. Straight, D.M., and Mehalic, C.M., "Performance Characteristics of an Afterburning Turbofan Engine with Steady-State Inlet-Flow Distribution", TM X-1898, August 1970, NASA. Confidential, Title (U).

10. Mehalic, C.M., and Lottig, R.A., "Steady-State Inlet Temperature Distortion Effects on the Stall Limits of a J85-GE-13 Turbojet Engine", TM X-2990, Feb. 1974, NASA.

11. Armentrout, E.C., "Development of a High-Frequency-Response Pressure-Sensing Rake for Turbofan Engine Tests", TMX-1959, Mar. 1970 NASA.

12. Alford, J.S., and Victor, I.W., "Dynamic Measurements of Forward Gas Expulsion During High Speed Stall of Jet Engines", SAE Paper 650840, Los Angeles, CA, 1965.

13, Mays, R.A., "Inlet Dynamics and Compressor Surge", Journal of Aircraft, Vol. 8, No. 4, April 1971, pp. 219-226.

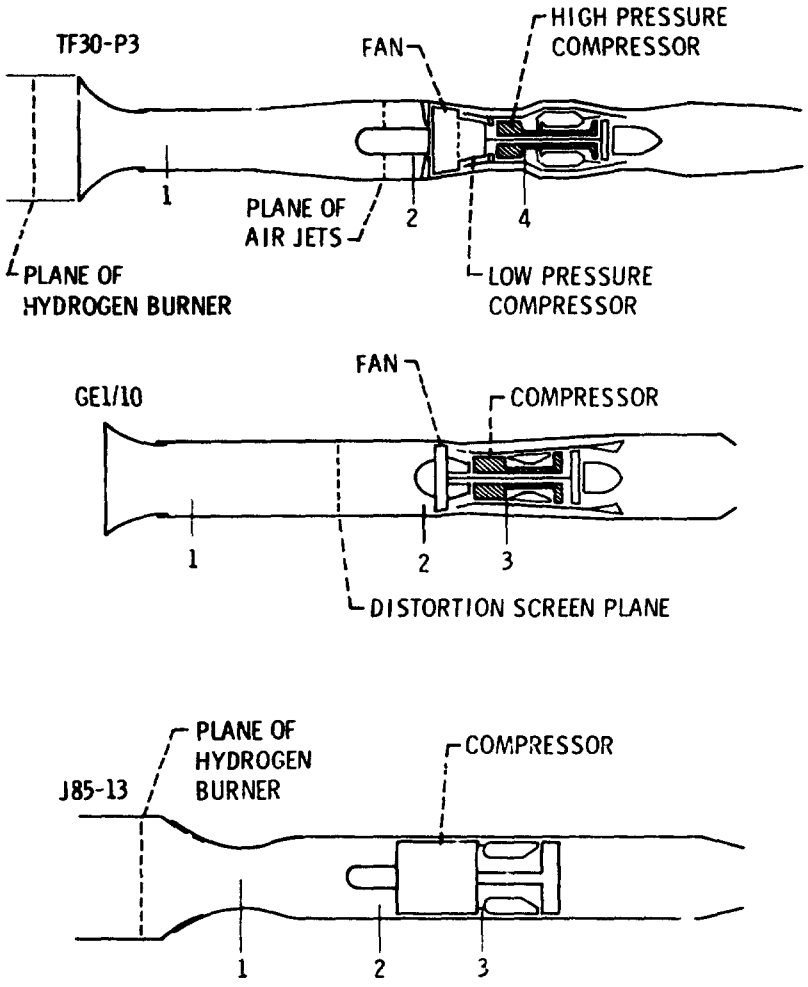

Figure 1. - Engines investigated.

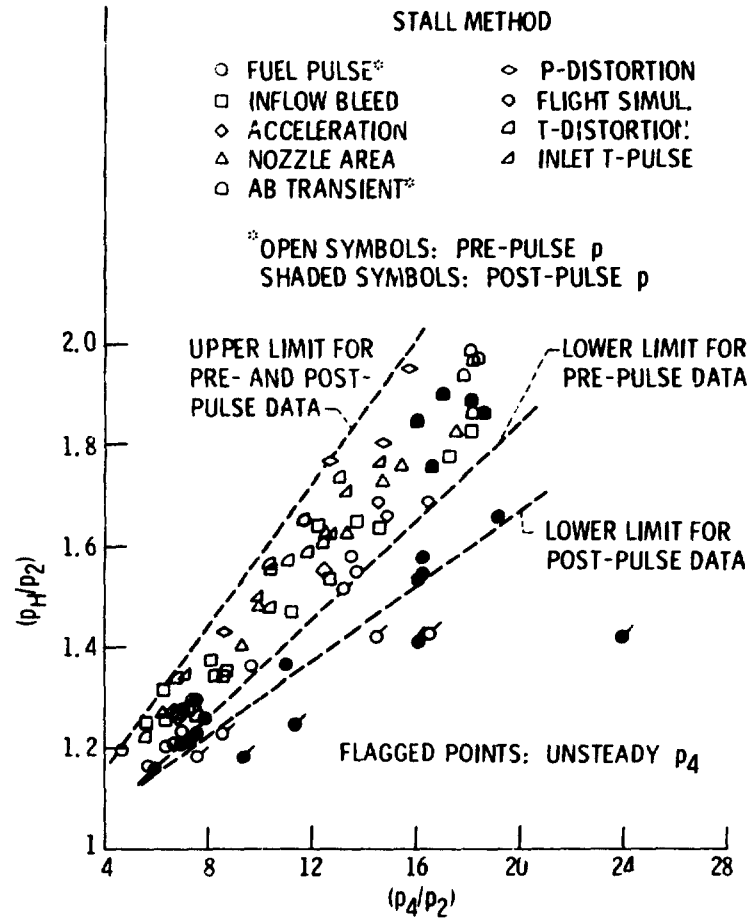

Figure 2. - Peak inlet static pressure ratio, TF30 engine.

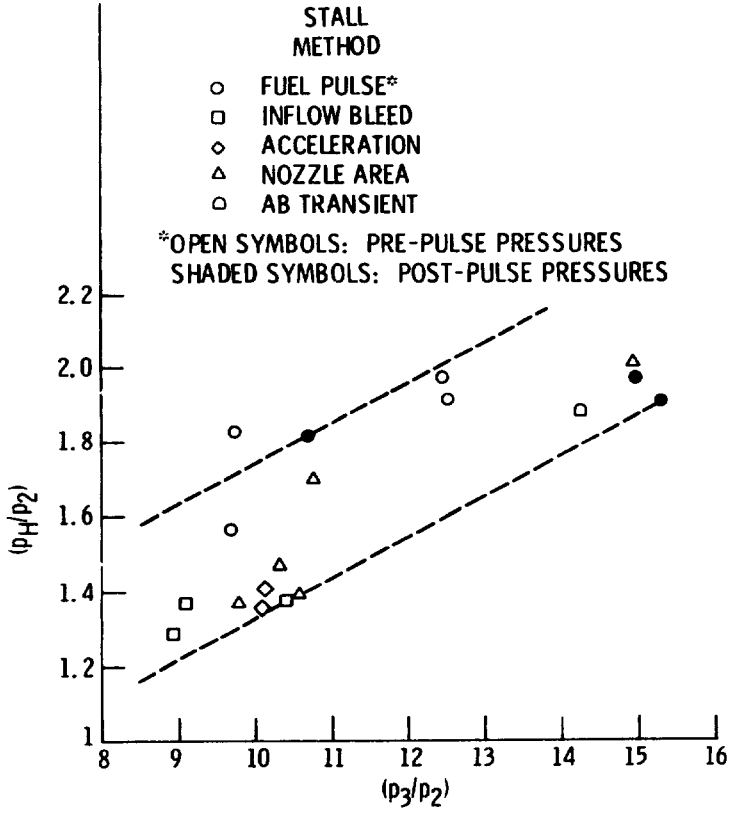

Figure 3. - Peak inlet static pressure ratio, GE 1/10 engine.

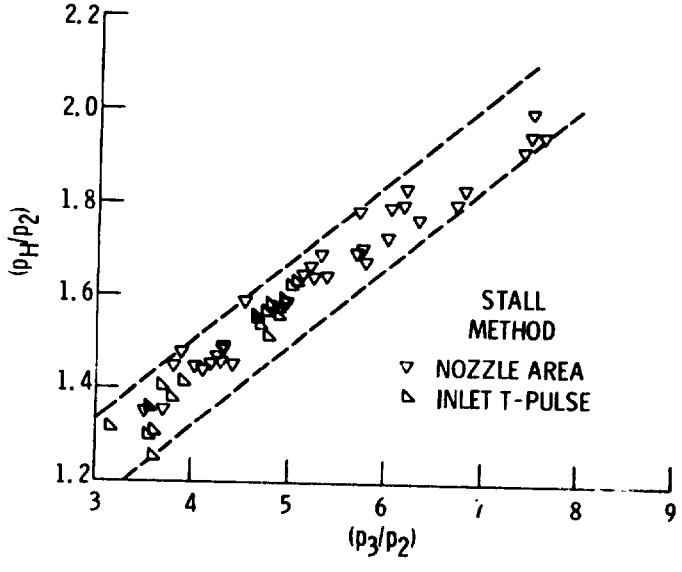

Figure 4. - Peak inlet static pressure ratio, J85 engine.

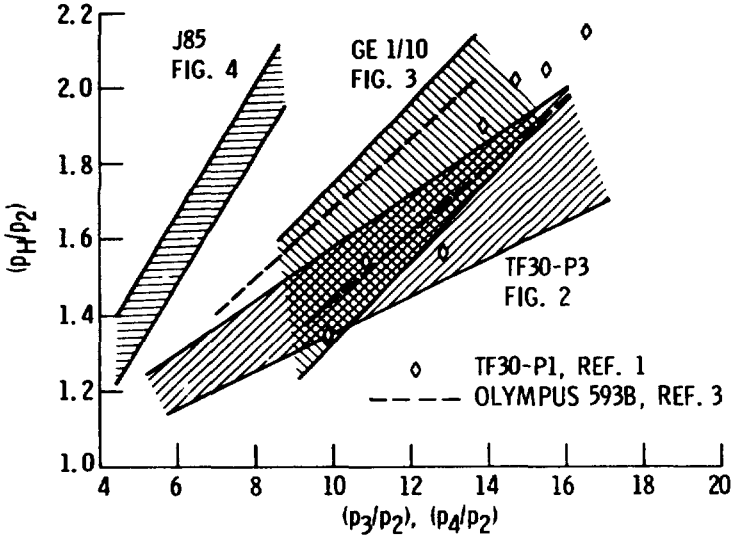

Figure 5. - Comparison of hammershock pressure ratios for several engines.

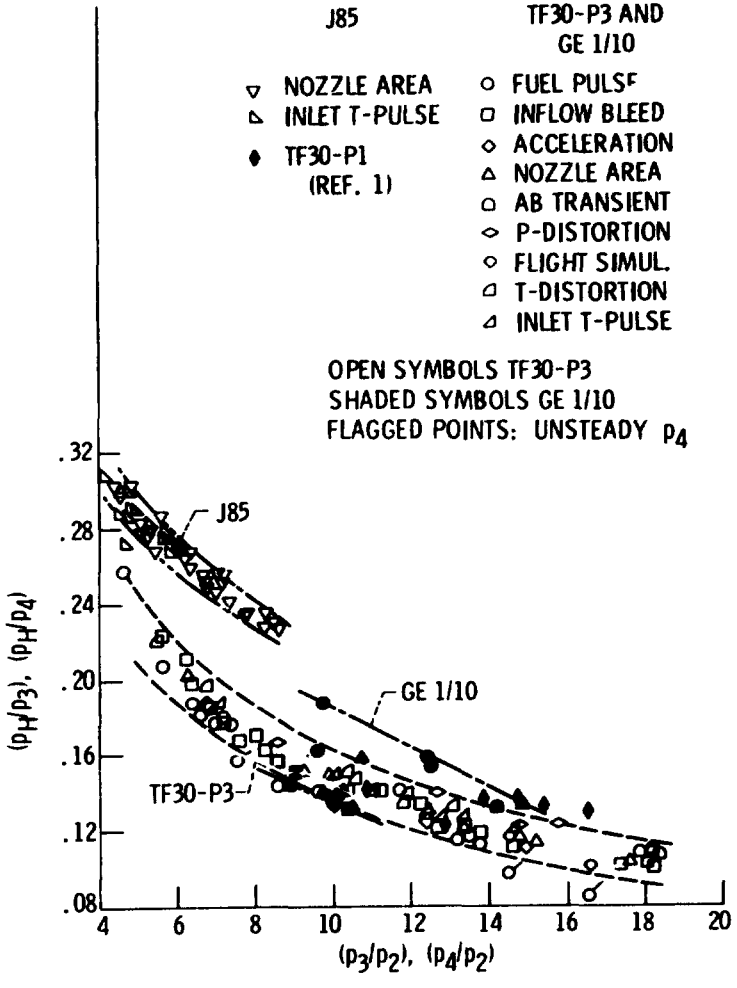

Figure 6. - Correlation of ratio of peak inlet to compressor exit pressure in terms of pressure ratio across the compressor.

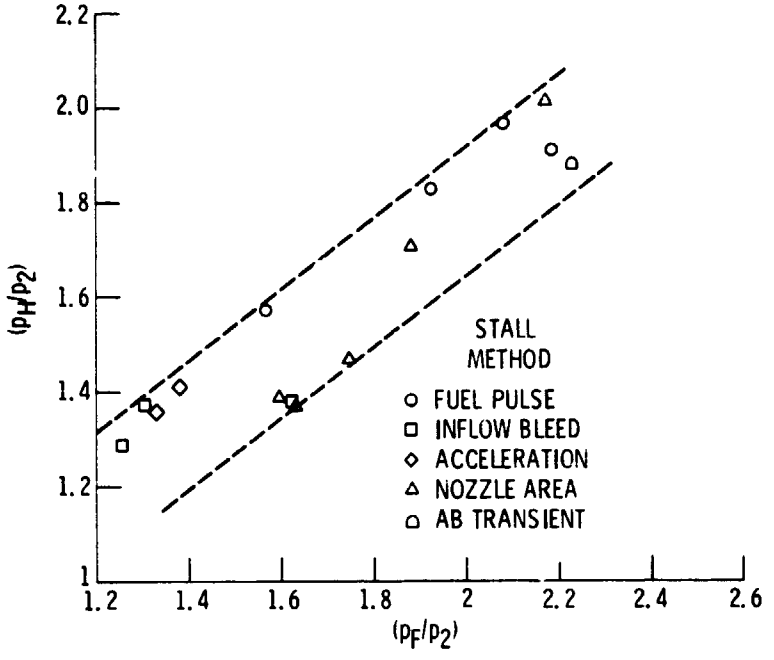

Figure 7. - Correlation of hammershock pressure ratio in terms of fan duct to engine inlet static pressure ratio, GE 1/10 engine.

E-8051

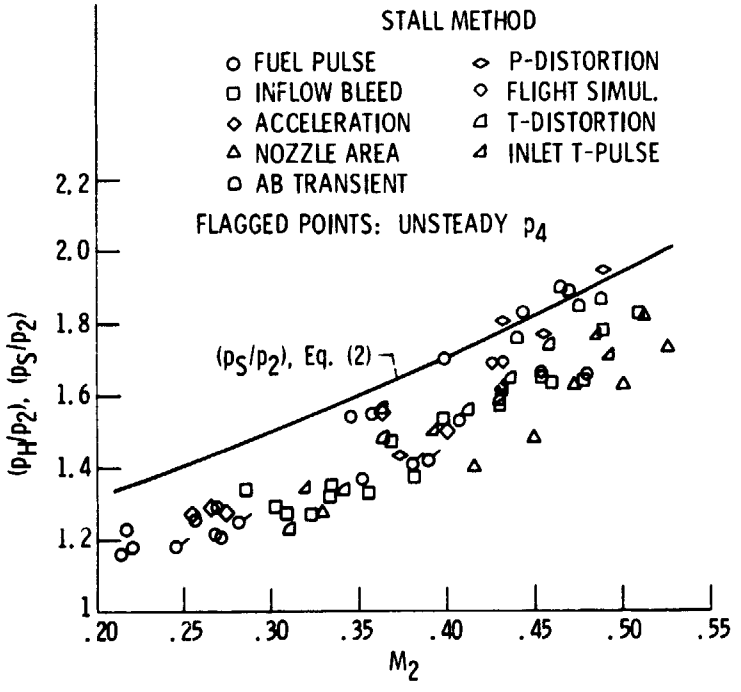

Figure 8. - Dependence of hammershock pressure ratio on engine inlet Mach number TF30 engine.

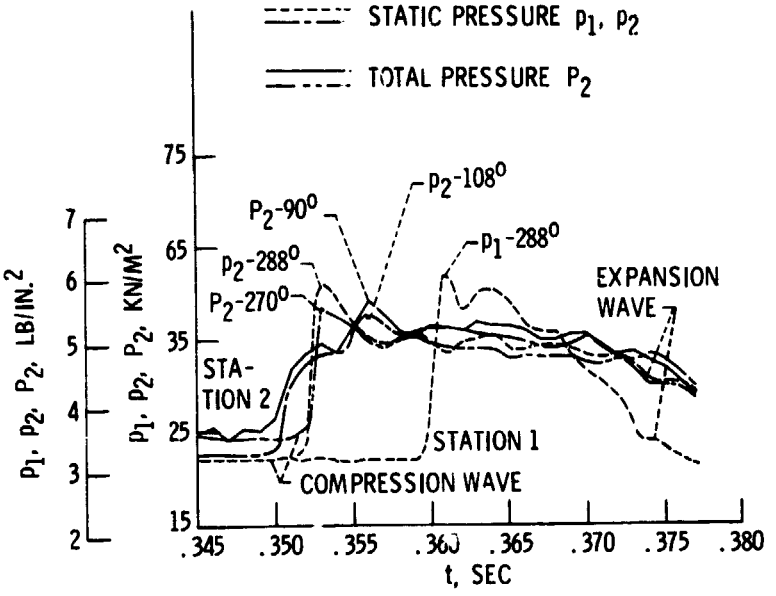

Figure 9. - Variation of total and static pressures at stations 1 and 2, TF30 engine.

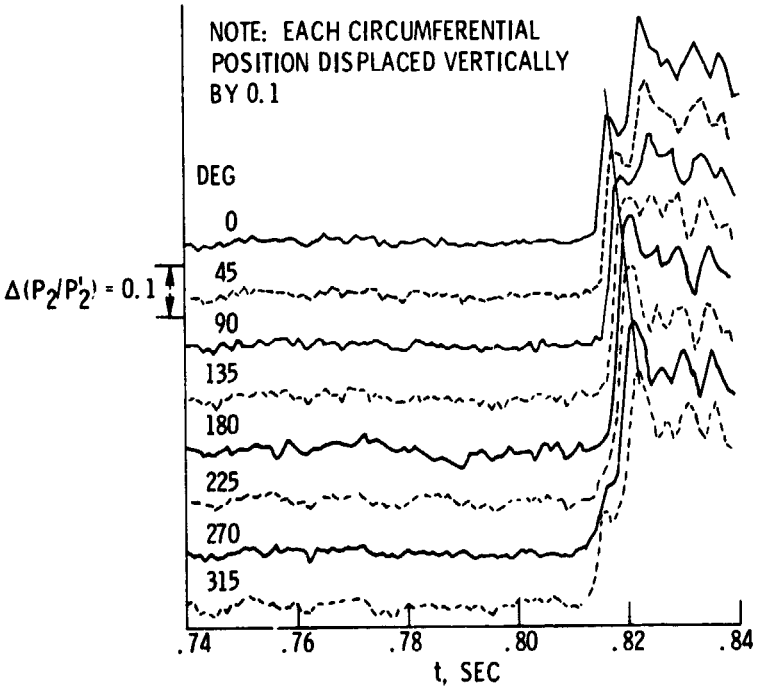

Figure 10. - Engine inlet total pressure histories during stall, TF30 engine.

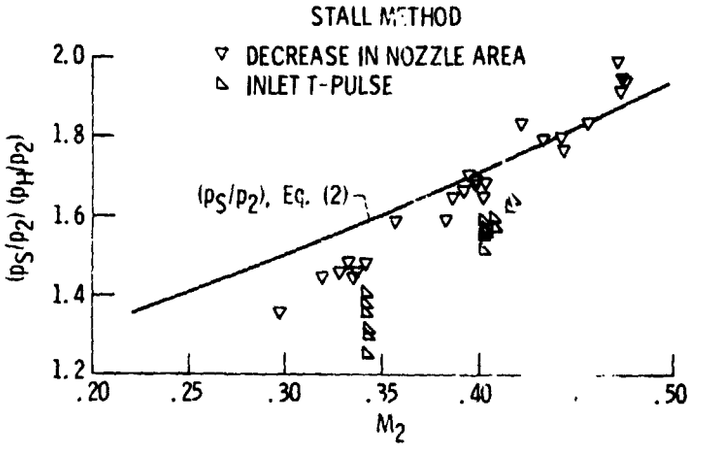

Figure 11. - Dependence of hammershock pressure ratio on engine inlet Mach number, J85 engine.

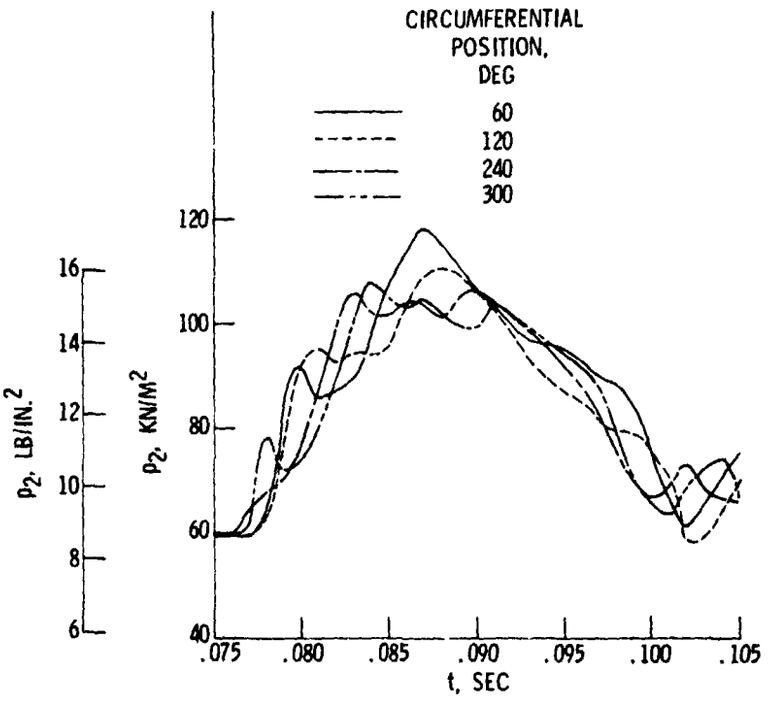

Figure 12. - Superimposed pressure histories at the engine inlet during stall, J85 engine.

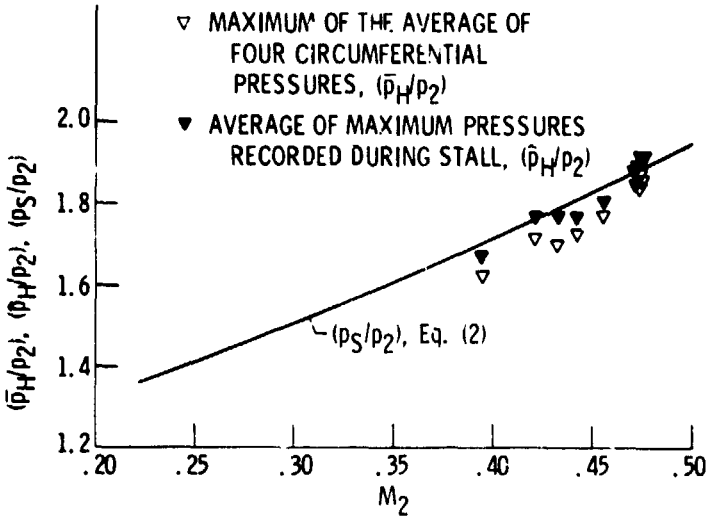

Figure 13. - Effect of pressure averaging on the hammershock pressure ratio, J85 engine.

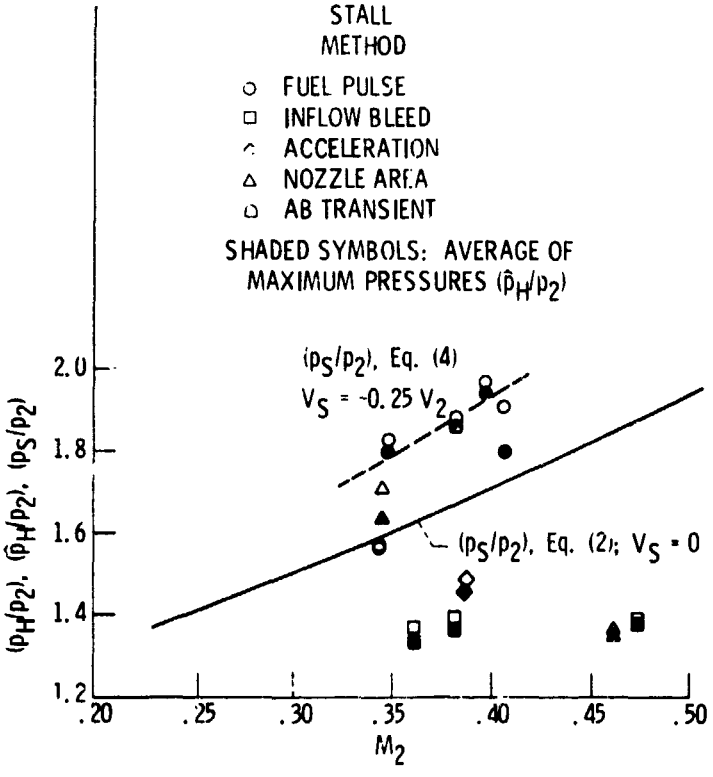

Figure 14. - Dependence of hammershock pressure ratio on engine inlet Mach number, GE 1/10 engine.

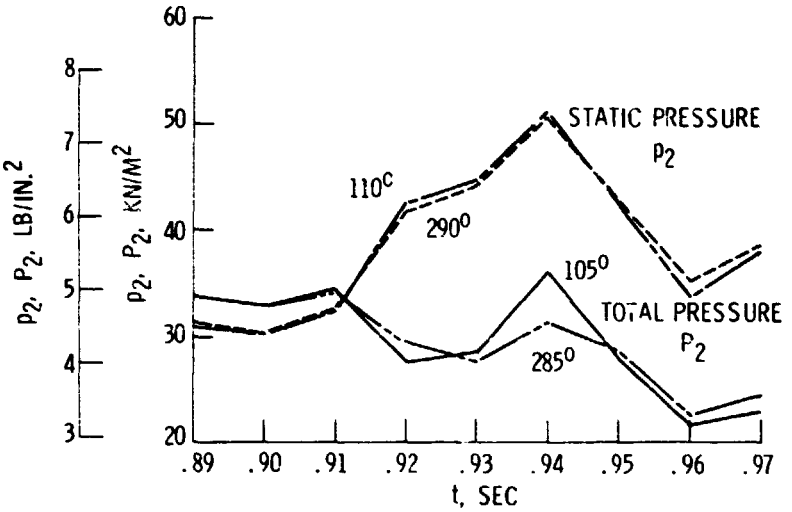

Figure 15. - Variation of total and static pressure at the engine inlet during stall, GE 1/10 engine.

E-8051

NASA-Lewis